Infinite Lifetime of Underwater Superhydrophobic States

Muchen Xu, Guangyi Sun, and Chang-Jin Kim*
Mechanical and Aerospace Engineering Department, University of California at Los Angeles (UCLA), Los Angeles, California 90095, USA

(Received 24 May 2014; revised manuscript received 21 July 2014; published 25 September 2014)

Submerged superhydrophobic (SHPo) surfaces are well known to transition from the dewetted to wetted state over time. Here, a theoretical model is applied to describe the depletion of trapped air in a simple trench and rearranged to prescribe the conditions for infinite lifetime. By fabricating a microscale trench in a transparent hydrophobic material, we directly observe the air depletion process and verify the model. The study leads to the demonstration of infinite lifetime (>50 days) of air pockets on engineered microstructured surfaces under water for the first time. Environmental fluctuations are identified as the main factor behind the lack of a long-term underwater SHPo state to date.

DOI: 10.1103/PhysRevLett.113.136103 PACS numbers: 68.08.Bc, 68.03.Cd, 68.35.Ct

The stability of the air layer on superhydrophobic (SHPo [1]) surfaces fully submerged in water is of critical importance because their key anticipated applications, such as drag reduction [2–5] and antibiofouling [6], are under water. Unfortunately, the air film on the underwater SHPo surface, often called a plastron, is fragile [2,7]. Over time, the air initially trapped on the SHPo surface diffuses away into the surrounding water, collapsing the air-water interface and causing a transition from the dewetted to wetted state [8]. Recent experimental studies showed that the lifetime of the underwater SHPo state is influenced by various environmental parameters [7,9–11]. However, most of the studies only reported statistical information, such as average wetting time; more direct knowledge, such as air-depletion dynamics or the effect of roughness geometries, is needed to design the SHPo surface to be more robust against wetting. While some underwater insects boast a long-term or even indefinite (tested up to 120 days [12]) plastron, all artificial SHPo surfaces retained their plastron for much shorter periods (mostly less than an hour; rarely, for days [7,9,13–15]). To date, no artificial SHPo surface has been demonstrated to retain an air layer indefinitely unless assisted [16].

This Letter aims to understand the air depletion process on submerged SHPo surfaces and to determine if an indefinite plastron is achievable. In order to systematically study the effect of geometric parameters of the surface structures for an intended goal, SHPo surfaces made of regular structures would be far more informative than those of random structures that produce only statistical data. Furthermore, for drag-reduction application in particular, SHPo surfaces with parallel trenches [3,4,17,18] have been found to outperform those with random structures [19,20], making SHPo surfaces with trenches a good candidate to study. Since multiple trenches are in parallel and isolated from each other, a single trench can represent the whole SHPo surface as far as the stability of the trapped air is concerned. The potential overestimation of the depletion speed on a single trench compared with the parallel trenches due to the edge effect [21,22] is considered minor to our goal. Instead, and which is important for our purpose, a sample with a single trench would allow clear images of one air-water meniscus; in comparison, multiple menisci in multiple trenches would overlap and blur the images. The transparent sample with a single trench was fabricated by hot embossing Teflon® fluorinated ethylene propylene (FEP) into a deep-reactive-ion-etch (DRIE)-processed silicon mold by improving the process from [23], as described in the Supplemental Material [24]. The whole Teflon® FEP sample is semiclear and intrinsically hydrophobic with advancing contact angle ~115° [28]. Figure 1(a) shows scanning electron microscopy (SEM) images of the single-trench sample. The sidewall of the trench has nanometer-scale roughness, as it was replicated from the "scalloped" surface [29] on the DRIE silicon mold.

Let us first analyze how the trapped air is depleted from a hydrophobic trench after being submerged based on previous works [15,30,31]. Consider a simple trench with

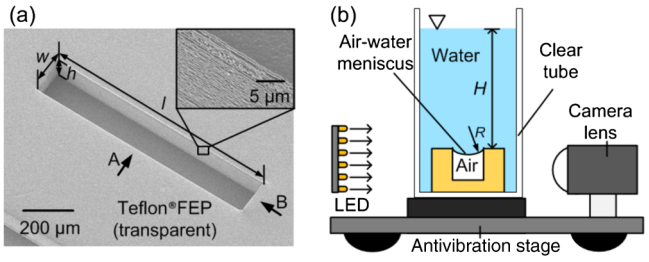

FIG. 1 (color online). The sample and testing setup. (a) SEM images of a single-trench sample with the microscale trench characterized by length l, width w, and depth h. (b) Schematic illustration of the experimental setup to visualize the air-water meniscus inside the trench throughout the depletion process. One sample was immersed in water of height H in a clear tube and observed from the side, as indicated by the arrow A in (a).

width w, length l, and depth h, as defined in Fig. 1(a), and the radius of curvature of the air-water interface R, as defined in Fig. 1(b). Since the trench length is much larger (~10 times) than its width, the meniscus was straight along the length of the trench in the middle section over a significant period of time before reaching the bottom, as shown in Fig. 2(a), supporting the 2D diffusion model as a crude but useful approximation. According to Henry's law, the partial pressure of a gas equilibrated in water is $p = k_H c$, where k_H is Henry's constant and c is the dissolved gas concentration in water. Right after submerging the sample from atmosphere (p_{atm}) to immersion depth H at hydrostatic pressure p_H, the air in the trench is compressed to $p_{tr,0}$ and the meniscus forms the radius of curvature R_0, as detailed in the Supplemental Material [24]. If $p_{tr,0} > k_H c$, air in the trench will start to diffuse out through the meniscus. The volume rate of dissolution (i.e., the dissolution rate) of the trapped air into the water is limited by the diffusion of dissolved air in the water, which is related to the temporal and spatial evolvement of concentration field by Fick's law, approximated [31] as

$$dV(t)/dt = -k_p A(t)[p_{tr}(t) - k_H c], \quad (1)$$

where V is the air volume, k_p is the mass transfer coefficient of air across the air-water interface, p_{tr} is the air pressure in the trench, and A is the meniscus area, or Eq. (S4) [24]. The influence of meniscus curvature on k_p was discussed in the Supplemental Material [24] based on diffusion-limited drop evaporation theory [32]. To estimate the value of k_p, diffusion length was eventually applied for simplicity [15], as explained in the Supplemental Material [24]. Combining Eq. (1) with the Laplace equation across the meniscus $p_{atm} + p_H - p_{tr} = \sigma/R$, where σ is the air-water interfacial tension, we get

$$\frac{dV(t)}{dt} = -k_p A(t)\left[p_H - \frac{\sigma}{R(t)} + p_{atm} - k_H c\right]. \quad (2)$$

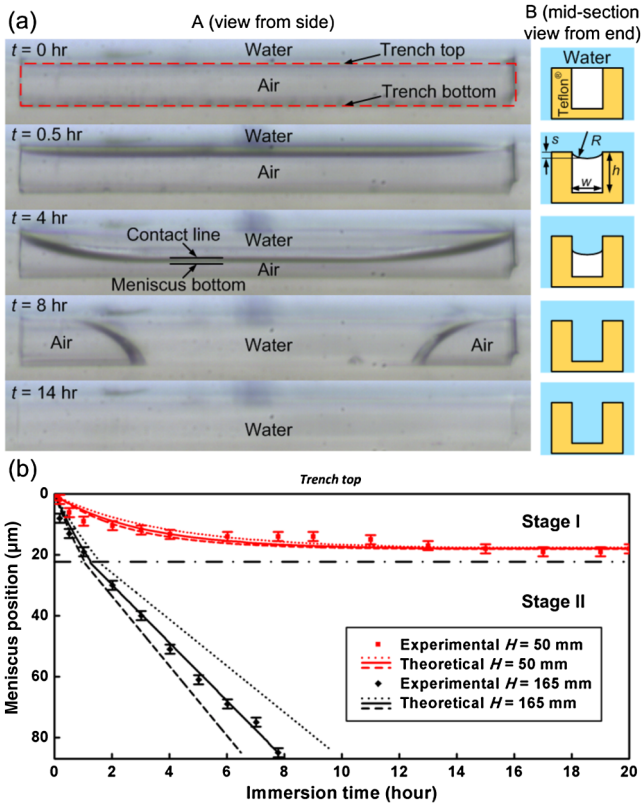

FIG. 2 (color online). Observed air depletion and trench wetting. (a) Air-water meniscus visualized by the setup shown in Fig. 1(b) with the viewing direction A shown in Fig. 1(a). Images from top to bottom show the meniscus starting to bend, depinning, sliding down, touching the trench bottom and fully wetting the trench. Shown on the right are the corresponding cross-sectional schematics with viewing direction B. For a complete movie, see Video S1 [24]. (b) Experimental and theoretical data of the meniscus position over time reveal two distinctive stability conditions, determined by the immersion depth H. The meniscus position is defined as the distance from the top edge of the trench to the lowest position of meniscus. Experimental data were obtained from continuous microscopy images of the air-water meniscus, as shown in Fig. 2(a), using samples with $w = 147$ μm, $h = 85$ μm, and $l = 1$ mm. Uncertainty of the position measurement (~ 3 μm) is shown in the Figure. Calculated for the same trench geometry and immersion depth, the solid line fit the data best with $k_p = 2.5 \times 10^{-12}$ cm/(sec·Pa), while the dotted lines show the influence of k_p with 2×10^{-12} m/(sec·Pa) and 3×10^{-12} m/(sec·Pa), respectively. The dot-dash line denotes the maximum deflection of the meniscus while the meniscus remained pinned at the top edge.

Here, we consider only depinning impalement (not sagging [33,34]) because the trench is much deeper than it is wide. The wetting process goes through two stages: (i) Stage I involves the contact line pinned to the top edge of the trench, and (ii) Stage II involves the contact line sliding on the sidewall of the trench. For the pinned stage of Stage I, R can be numerically calculated with initial condition R_0 and boundary condition R_c, as detailed in the Supplemental Material [24]. Since the depinning occurs when the angle of the meniscus on the sidewall reaches the advancing contact angle θ_{adv} [33], $R_c = w/2\cos\theta_{adv}$. For the sliding stage of Stage II, since $R = R_c =$ constant for the simple trench, the meniscus slides down the vertical sidewall at constant speed $u = d(V/A)/dt$, which can also be obtained from Eq. (2). The meniscus movement was estimated from video recordings, such as Video S1 [24], assuming a smooth sidewall. The scallops on the sidewalls were too small (~500 nm apart) to appear in the optical images [e.g., Fig. 2(a)] used for the measurement. If diffusion rate $dV(t)/dt$ can decrease to zero during the pinned stage (Stage I), the meniscus will reach a stable state and the air loss will cease. However, once the meniscus depins and

proceeds to the sliding stage (Stage II), the meniscus curvature and pressure p_{tr} will not change further. Defined as the maximum immersion depth beyond which the air-water meniscus has no stable state, the critical immersion depth H_c is the depth where air diffusion rate decreases to zero at the end of Stage I. By substituting $dV(t)/dt = 0$ and $R = R_c = w/2\cos\theta_{adv}$ into Eq. (2), we obtain

$$H_c = \frac{2\sigma\cos\theta_{adv}}{w\rho g} + \frac{k_H c - P_{atm}}{\rho g}, \quad (3)$$

where ρ is the density of water and g is the gravitational acceleration. Note that $k_H c - p_{atm}$ is the difference between the pressures of the dissolved air at the immersion depth and the atmospheric air just above the water. If the dissolved air is in full equilibrium with the atmosphere so that $k_H c - p_{atm} = 0$, Eq. (3) reduces to the well-known relation below [35]:

$$H_c = \frac{2\sigma\cos\theta_{adv}}{w\rho g}. \quad (4)$$

Assuming equilibrium, Eq. (4) simply states that the critical immersion depth is when the hydrostatic pressure at the depth equals the Laplace pressure sustainable by the interface at the trench. In contrast, Eq. (3) further specifies how the critical immersion depth is affected when the condition diverges from the equilibrium. Because the environmental parameters (e.g., temperature, atmospheric pressure) keep changing in reality, the dissolved air at the immersion depth is always in the process of equilibrating through diffusion, so $k_H c - p_{atm} \neq 0$ in reality. The above analysis is based on a single component gas but still applies to multiple-component gases (e.g., air), because partial volumes and partial pressures can be added up in Eq. (1).

In order to elucidate the dynamic process of air depletion and trench wetting, a setup was developed to directly visualize the meniscus, as schematically illustrated in Fig. 1(b). Unlike the confocal-microscopy-based [7,15,33] studies, a cool LED (NuGreen Flexible Neck LED Desk Lamp, Newer Technology) was used as the light source to allow long-term observation without heating. As shown in Fig. 2(a), curved across the width of the trench, the meniscus appears as a dark strip, whose upper border is the two contact lines on the two sidewalls and whose lower border is the lowest position between the two sidewalls. When the sample was just immersed in water, the meniscus was almost flat and pinned at the top edges of the trench, as shown in the image at $t = 0$ hr. At $t = 0.5$ hr, the meniscus bent down as some of the trapped air diffused out, but the meniscus was still pinned to the top edges. As more air diffused out, the meniscus continued to bend down until finally depinning from the top edges and moving down the sidewall, as shown in the image at $t = 4$ hr. When the meniscus touched the bottom of the trench, the meniscus split into two and spread rapidly towards the ends to satisfy the local contact angle, forming convex along the trench length and concave along the trench width. The spreading slowed down as the spreading menisci started to compress the air trapped at the corners, as suggested by the curvature change of the contact line. The trapped air continued to diffuse into the water and disappeared eventually, as shown in Video S1 in the Supplemental Material [24]. In this study, we define the "lifetime" of the trapped air in the trench as the time between the moment of immersion and the moment of the meniscus touching the trench bottom. However, this definition should not be considered universal. For SHPo drag reduction, as an example, the time to the meniscus depinning, after which the designed reduction is compromised, may define the lifetime better.

In Fig. 2(b), the meniscus movement shown in Fig. 2(a) was quantified for a sample immersed at two different depths. For small immersion depth (i.e., $H = 50$ mm), the meniscus bent down and stayed relatively stable, remaining in Stage I for many hours. However, for large immersion depth (i.e., $H = 165$ mm), the meniscus bent down, depinned, moved down, and touched the bottom. The meniscus position decreased faster at the beginning during Stage I but slowed down to a constant speed (i.e., linear trend) during Stage II. The lines are drawn from Eq. (2) with $k_H c - P_{atm} = 0$, which are consistent with [31], using R_0 and k_p derived and using θ_{adv} measured in the Supplemental Material [24]. In addition to helping us define the lifetime, the results in Fig. 2 confirm the theoretical model based on two stages of wetting and suggest the existence of stable menisci, i.e., infinite lifetime.

If only lifetime data of the air pocket are needed without the depletion dynamics above, the setup can be simplified by placing the sample sideways and observing the trench from above its opening with a low-magnification camera, as schematically illustrated in Fig. S2 in the Supplemental Material [24]. Three exemplary images captured from a video clip are shown in Fig. 3(a). The total reflection of the light from behind the sample made the meniscus in the trench appear darker to the camera, compared with the rest of the sample. These observations were confirmed to be consistent with the detailed dynamics of Fig. 2, validating the simplified setup, which allowed us to monitor multiple samples simultaneously and continuously in a controlled environment, as detailed in the Supplemental Material [24].

Figure 3(b) shows the lifetime of the trapped air of multiple samples tested at varying immersion depths. All samples ($10 \times 5 \times 0.5$ mm Teflon® FEP piece) have one trench with the same length ($l = 1$ mm) and depth ($h \sim 85$ μm), but three different widths. For all three trench widths the lifetime increased as the immersion depth decreased, which is consistent with Eq. (3) and previous experimental results [7,13,15]. However, when

the immersion depth was smaller than a certain value, the trench retained the air pocket for a very long time. We declared the lifetime "infinite" after 1200 hours (50 days) and terminated the recording, but some tests were left to continue with no sign of wetting. For each trench width, the critical immersion depth H_c should be between the last data (i.e., the smallest depth) among those that became wet and the first data (i.e., largest depth) that showed an indefinite lifetime, indicating the uncertainty of measuring instability data. As shown in Fig. 3(c), the experimentally obtained ranges of H_c matched the theoretical reciprocal curve based on Eq. (4). As expected, trenches with a smaller width can be submerged deeper without losing the air pocket. Since the environmental fluctuation cannot be completely eliminated, the experimental data are slightly smaller (i.e., shallower) than the theoretically predicted depth in Fig. 3(c).

To the best of our knowledge, this is the first experimental verification of infinite lifetime of entrapped gas

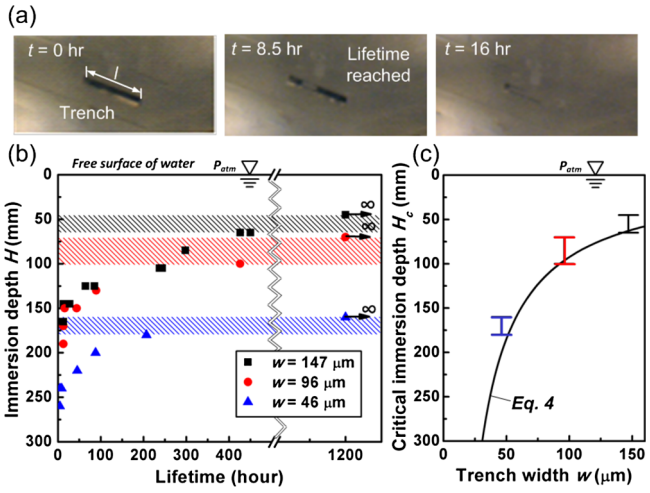

FIG. 3 (color online). Observed lifetime of trapped air. (a) Air-water meniscus seen from above the sample with low-magnification camera. The meniscus appears black. The black strip at $t = 0$ hr, the broken strip at $t = 8.5$ hr, and the disappearance of the strip at $t = 16$ hr indicate the beginning, touching bottom, and full wetting, respectively, corroborating the observation in Fig. 2(a). (b) Lifetime of trapped air as a function of immersion depth with trench width of 147 μm (closed square), 96 μm (closed circle), and 46 μm (closed triangle) as the parameter. The measurement errors of immersion depth (i.e., ± 2.5 mm due to evaporation, as explained in the Supplemental Material [24]) and lifetime (i.e., the interval between snapshots) are too small to appear in the given scales. The symbols with an arrow indicate at least 1200 hours, considered infinite in this study. Each of the three colored shades indicates the uncertainty range of critical depth H_c for a given trench width. (c) Critical immersion depth H_c as a function of trench width w. The experimental results are from the uncertainty ranges (i.e., the colored shades) in (b). The solid line is the theoretical prediction of Eq. (4) with 130° as the advancing contact angle measured on the trench sidewall (obtained in the Supplemental Material [24]).

on microstructured surfaces fully submerged in water. Compared with previous tests, we note several aspects critical to our success. (1) The surface should be tested at a smaller depth than the critical immersion depth. However, this basic requirement was not always met before (e.g., [15]). (2) The samples in this Letter had a simple and distinctive geometry and were carefully examined to avoid any defect. Assuming a similar dimensional scale, an ordered structure is favored over random structures [7,13,14] because the latter get wetted more easily, as discussed in the Supplemental Material [24]. (3) Made entirely of Teflon® FEP, the samples in this Letter did not need any hydrophobic coating, which is a typical source of defects for SHPo surfaces. Many used a self-assembled monolayer [14,15,35], which was found to degrade under water over time [36]. (4) The experimental procedure was carefully controlled and environmental fluctuations minimized, as detailed in the Supplemental Material [24]. This extreme care was especially important when the testing depth was close to the theoretical limit.

In summary, we applied a theoretical model to describe the depletion dynamics and rearranged it to prescribe the stable state of the air trapped in a simple hydrophobic trench under water. Then we verified the model through direct observation of air-water meniscus and experimentally obtained a stable air pocket in the trench. The lifetime of the air pocket was obtained as function of immersion depth with the trench width as a parameter. The infinite lifetime (>1200 hours) was obtained by minimizing the environmental fluctuations in the experiments. The critical immersion depth, within which the indefinite plastron is possible, was confirmed to depend reciprocally on the trench width. While verifying that the indefinite plastron can exist as predicted by the theoretical model, this study conversely attests to the delicate fragility of the plastron on SHPo surfaces. To keep a plastron stable under realistic conditions, where environmental parameters would fluctuate significantly, one should use the SHPo surface at a much shallower depth than the theoretical critical immersion depth. Although performed under a near-thermodynamic-equilibrium environment far from realistic conditions, this study nevertheless teaches us (1) that the indefinite SHPo state does exist, (2) how to design SHPo surfaces to retain the air better, and (3) that the indefinite SHPo state would not be possible for many applications unless energetically assisted [16]. In particular for drag reduction, which requires a trench width larger than ~ 20 μm [18], the results indicate long-term (e.g., days) operations are not possible in field conditions unless the immersion is very shallow (e.g., mere centimeters) or the gas is replenished [16].

This work has been supported by the ONR Grant No. N000141110503 and NSF Grant No. 1336966. The authors thank Ryan Freeman for help with the manuscript.

*cjkim@ucla.edu

[1] We abbreviate superhydrophobic to SHPo in order to differentiate it from superhydrophilic (SHPi) as well as the likes of superlyophobic and superoleophobic.

[2] L. Bocquet and E. Lauga, Nat. Mater. **10**, 334 (2011).

[3] C. Lee, C.-H. Choi, and C.-J. Kim, Phys. Rev. Lett. **101**, 064501 (2008).

[4] R. J. Daniello, N. E. Waterhouse, and J. P. Rothstein, Phys. Fluids **21**, 085103 (2009).

[5] E. Karatay, A. S. Haase, C. W. Visser, C. Sun, D. Lohse, P. A. Tsai, and R. G. H. Lammertink, Proc. Natl. Acad. Sci. U.S.A. **110**, 8422 (2013).

[6] K. Koch and W. Barthlott, Phil. Trans. R Soc. A **367**, 1487 (2009).

[7] R. Poetes, K. Holtzmann, K. Franze, and U. Steiner, Phys. Rev. Lett. **105**, 166104 (2010).

[8] Y. H. Xue, S. G. Chu, P. Y. Lv, and H. L. Duan, Langmuir **28**, 9440 (2012).

[9] W.-Y. Sun and C.-J. Kim, in *Proceedings of the IEEE International Conference on Micro Electro Mechanical Systems (MEMS)* (IEEE, Piscataway, NJ, 2013), p. 397.

[10] M. A. Samaha, H. V. Tafreshi, and M. Gad-el-Hak, Langmuir **28**, 9759 (2012).

[11] F. O. Ochanda, M. A. Samaha, H. V. Tafreshi, G. C. Tepper, and M. Gad-el-Hak, J. Appl. Polym. Sci. **124**, 5021 (2012).

[12] A. Balmert, H. Florian Bohn, P. Ditsche-Kuru, and W. Barthlott, J. Morphol. **272**, 442 (2011).

[13] M. A. Samaha, H. V. Tafreshi, and M. Gad-el-Hak, Phys. Fluids **24**, 112103 (2012).

[14] M. S. Bobji, S. V. Kumar, A. Asthana, and R. N. Govardhan, Langmuir **25**, 12120 (2009).

[15] P. Lv, Y. Xue, Y. Shi, H. Lin, and H. Duan, Phys. Rev. Lett. **112**, 196101 (2014).

[16] C. Lee and C.-J. Kim, Phys. Rev. Lett. **106**, 014502 (2011).

[17] B. Woolford, J. Prince, D. Maynes, and B. W. Webb, Phys. Fluids **21**, 085106 (2009).

[18] H. Park, G. Sun, and C.-J. Kim, J. Fluid Mech. **747**, 722 (2014).

[19] E. Aljallis, M. A. Sarshar, R. Datla, V. Sikka, A. Jones, and C. H. Choi, Phys. Fluids **25**, 025103 (2013).

[20] C.-H. Choi and C.-J. Kim, Phys. Rev. Lett. **96**, 066001 (2006).

[21] F. Scholz, *Electroanalytical Methods: Guide to Experiments and Applications* (Springer, New York, 2009).

[22] R. D. Deegan, O. Bakajin, T. F. Dupont, G. Huber, S. R. Nagel, and T. A. Witten, Nature (London) **389**, 827 (1997).

[23] K. N. Ren, W. Dai, J. H. Zhou, J. Su, and H. K. Wu, Proc. Natl. Acad. Sci. U.S.A. **108**, 8162 (2011).

[24] See Supplemental Material at http://link.aps.org/supplemental/10.1103/PhysRevLett.113.136103, which includes Refs. [25–27].

[25] E. L. Cussler, *Diffusion: Mass Transfer in Fluid Systems* (Cambridge University Press, Cambridge, England, 2009).

[26] P. B. Duncan and D. Needham, Langmuir **20**, 2567 (2004).

[27] T. Enns, P. F. Scholander, and E. D. Bradstreet, J. Phys. Chem. **69**, 389 (1965).

[28] W. Feast, H. Munro, and R. W. Richards, *Polymer Surfaces and Interfaces II* (Wiley, New York, 1993), Vol. 2.

[29] M. J. Madou, *Fundamentals of Microfabrication: The Science of Miniaturization* (CRC Press, Boca Raton, Florida, 2002).

[30] M. Flynn and J. W. Bush, J. Fluid Mech. **608**, 275 (2008).

[31] B. Emami, A. Hemeda, M. Amrei, A. Luzar, M. Gad-el-Hak, and H. V. Tafreshi, Phys. Fluids **25**, 062108 (2013).

[32] R. Picknett and R. Bexon, J. Colloid Interface Sci. **61**, 336 (1977).

[33] P. Papadopoulos, L. Mammen, X. Deng, D. Vollmer, and H.-J. Butt, *Proc. Natl. Acad. Sci. U.S.A.* 110, 3254 (2013).

[34] M. Reyssat, J. M. Yeomans, and D. Quere, Europhys. Lett. **81**, 26006 (2008).

[35] H. Rathgen and F. Mugele, Faraday Discuss. **146**, 49 (2010).

[36] B. Kobrin, J. Chin, and W. Ashurst, in *World Tribology Congress III* (American Society of Mechanical Engineers, Washington, DC, USA, 2005), p. 533.